


Review

A Review on Impedimetric and Voltammetric Analysis Based on Polypyrrole Conducting Polymers for Electrochemical Sensing Applications

Nurul Akmaliah Dzulkurnain ¹, Marliyana Mokhtar ², Jahwarhar Izuan Abdul Rashid ¹ , Victor Feizal Knight ², Wan Md Zin Wan Yunus ³, Keat Khim Ong ², Noor Azilah Mohd Kasim ² and Siti Aminah Mohd Noor ^{1,*}

¹ Department of Chemistry and Biology, Centre for Defence Foundation Studies, National Defence University of Malaysia, Sungai Besi Camp, Kuala Lumpur 57000, Malaysia; nurulakmaliah86@gmail.com (N.A.D.); jahwarhar@upnm.edu.my (J.I.A.R.)

² Research Centre for Chemical Defence, National Defence University of Malaysia, Sungai Besi Camp, Kuala Lumpur 57000, Malaysia; marliyanamokh@yahoo.com (M.M.); victor.feizal@upnm.edu.my (V.F.K.); ongkhim@upnm.edu.my (K.K.O.); azilah@upnm.edu.my (N.A.M.K.)

³ Centre for Tropicalisation, National Defence University of Malaysia, Sungai Besi Camp, Kuala Lumpur 57000, Malaysia; wanmdzin@upnm.edu.my

* Correspondence: s.aminah@upnm.edu.my



Citation: Dzulkurnain, N.A.; Mokhtar, M.; Rashid, J.I.A.; Knight, V.F.; Wan Yunus, W.M.Z.; Ong, K.K.; Mohd Kasim, N.A.; Mohd Noor, S.A. A Review on Impedimetric and Voltammetric Analysis Based on Polypyrrole Conducting Polymers for Electrochemical Sensing Applications. *Polymers* **2021**, *13*, 2728. <https://doi.org/10.3390/polym13162728>

Academic Editor: Jung-Chang Wang

Received: 7 June 2021

Accepted: 27 July 2021

Published: 15 August 2021

Publisher's Note: MDPI stays neutral with regard to jurisdictional claims in published maps and institutional affiliations.



Copyright: © 2021 by the authors. Licensee MDPI, Basel, Switzerland. This article is an open access article distributed under the terms and conditions of the Creative Commons Attribution (CC BY) license (<https://creativecommons.org/licenses/by/4.0/>).

Abstract: Conducting polymers have been widely used in electrochemical sensors as receptors of the sensing signal's analytes and transducers. Polypyrrole (PPy) conducting polymers are highlighted due to their good electrical conductive properties, ease in preparation, and flexibility of surface characteristics. The objective of this review paper is to discuss the theoretical background of the two main types of electrochemical detection: impedimetric and voltammetric analysis. It also reviews the application and results obtained from these two electrochemical detections when utilizing PPy as a based sensing material in electrochemical sensor. Finally, related aspects in electrochemical sensor construction using PPy will also be discussed. It is anticipated that this review will provide researchers, especially those without an electrochemical analysis background, with an easy-to-understand summary of the concepts and technologies used in electrochemical sensor research, particularly those interested in utilizing PPy as a based sensing material.

Keywords: electrochemical sensor; biosensor; impedimetric; voltammetric; polypyrrole; conducting polymer

1. Introduction

Conducting polymers (CPs) play an important role in the design and development of electrochemical sensors. They provide the necessary electrical conductivity to transduce the occurrence of the coupling event into an analytical signal (Figure 1) [1].

CPs are conjugated polymers that possess delocalized π -bonds on the backbone of the polymers. These π -bonds assist in the migration of electrons throughout the polymeric chain. Thus, these polymers can act as conductors, semiconductors, or even superconductors. Besides that, CPs also have high electron affinity and redox activity. The general physical properties of CPs depend on the size and length of the conducting polymer, which can also be described in terms of their molecular weight [2]. There are many types of CPs such as polyaniline (PANI), polypyrrole (PPy), polyacetylene, polyparaphenylene (PPPh), polyparaphenylene vinylene (PPV), polythiophenes (PTh), polydiaminonaphthalene, polyazulene, and poly (3,4-ethylene dioxythiophene) (PEDOT) [3]. Electrically conductive polymers are a class of materials that can be fabricated to generate either transient or static electrical charges because of their physico-chemical properties [4]. Among those polymers, PPy is the most extensively used as a conducting polymer in electrochemical sensing applications because it is a heterocyclic conducting polymer, with good

environmental stability, high electronic conductivity, and biocompatibility compared to other CPs [5–8].

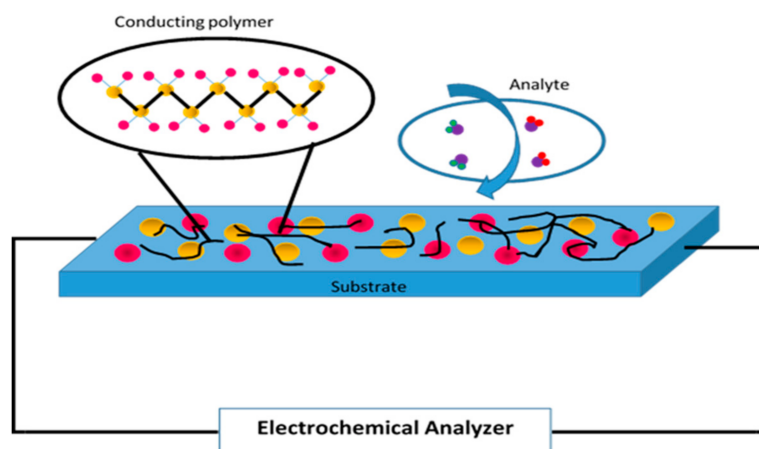


Figure 1. Schematic diagram of a conducting polymer and analyte on an electrochemical sensor.

Furthermore, PPy is easy to synthesize as a black powder chemically and electrochemically as thin films on various electrodes for both aqueous and nonaqueous media [4,9–11]. PPy has also been applied in multidisciplinary applications such as batteries, supercapacitors, coatings, etc. [12–14]. Despite these excellent properties, it also suffers from certain drawbacks, namely, poor thermal solubility and low mechanical stability [15]. These drawbacks can affect the response characteristics and sensitivity to small perturbation of the electrochemical sensor [3]. In the past two decades, scientists have applied different approaches to modifying PPy to improve its properties. These approaches include blending [16], electro-polymerization [17], interpenetrating network formation, and composite synthesis [18,19].

1.1. Synthesis and Preparation of Polypyrrole

PPy is commonly synthesized through chemical or electrochemical oxidation of pyrrole monomer using oxidant agents through a conjugated bond system with the polymer backbone. However, in the presence of only PPy, it may suffer from a certain drawback as mentioned above, and this will restrict the device's application. Therefore, approaches such as blending, electro-polymerization, interpenetrating network formation, and composite synthesis have been done to enhance the PPy properties, thus improving the device's performance.

Hosseini and Entezami, 2003, prepared the polymer by blending PPy with polyvinyl acetate (PVAc), polystyrene (PS), and polyvinyl chloride (PVC) using a chemical method to produce flexible and free-standing blended polymer films. The sensing abilities of these films towards toxic gases and vapors were investigated and it was discovered that the PPy blended film had improved mechanical strength and was also able to exhibit greater environmental stability. Besides that, it was also found the sensoric properties of the PPy blends towards toxic gases and vapors against hydrogen halides, hydrogen cyanide, and halomethyl compounds were better than non-blended PPys. Therefore, it can be surmised from their findings that PPy blends are good candidates for sensing toxic gases and vapors [16].

Meanwhile, Song et al., 2019, prepared three-dimensional graphene oxide with an interconnected porous polypyrrole (pGO/PPy) nanostructure-based actuator through electro-polymerization and sonication. This configuration allowed the actuator to adsorb trace cadmium by the carboxyl functional group in the GO and also was able to widen the electrode detection range of the PPy which was densely covered with gold substrate. From the results obtained, they suggest that the pGO/PPy was a promising material that had an ability to enhance the pre-concentration factors, enrich the potential window and

greatly increase the sensitivity of the cadmium sensor. The cadmium detection in the presence of interference ions showed good selectivity using this pGO/PPy nanostructure based actuator. Besides which, the nanostructure also achieved a wider linear range and a lower limit of detection (LOD). Moreover, this method could be developed into a low cost, portable and reliable sensor that is both sensitive and selective towards cadmium in aqueous systems and could potentially facilitate detection of other heavy metals such as lead, mercury and copper [17].

Hassanein et al., 2017, fabricated biosensors based on chitosan-ZnO/Polypyrrole nanocomposites. The sensor was prepared using the oxidative polymerization of pyrrole monomer with $(\text{NH}_4)_2\text{S}_2\text{O}_8$ as the oxidant and followed by mixing with chitosan-zinc oxide composites. The conductive polymers and oxide nanoparticles (organic-inorganic nanocomposite materials) have been previously widely used because of the novel properties of this nanocomposite which can be attributed to the successful blending of the individual characteristics of the parent constituents into a single material. The advantages of the oxide nanoparticles are in their ability to modify their chemical, mechanical, electrical, structural, morphological, and optical properties under specific circumstances. Moreover, these nanostructure materials have a larger percentage of surface atoms available which possess high reactivity. From the results, it was found that there was a significant improvement in electrical conductivity from the cyclic voltammetry measurements of the $\text{K}_3(\text{Fe}(\text{CN})_6)$ sample. A large enhancement of the stripping of peak current compared to bare CPE was identified using the square-wave adsorptive anodic stripping voltammetry method. Consequently, the proposed material proved to possess suitable ability as sensing materials in biosensor applications [18].

In other work done by Tlili et al., 2005, they reported the technique of interpenetrating network formation, where they immobilized DNA probes bearing amine groups by covalent grafting on a supporting polypyrrole matrix functionalized with activated ester groups. The immobilization step played an important role in determining the overall performance of the biosensor. In order to achieve high sensitivity and selectivity, it required minimization of non-specific adsorption and stability of the immobilization. Polypyrrole (PPy) conducting polymer was chosen in their study because of its biocompatibility, high hydrophilic character combined with high stability in water and facile incorporation of many counter ions which make it highly suitable as an interface for grafting DNA probes onto a micro-sized surface. From the results, it was discovered that the large surface area obtained by using porous polypyrrole leads to an increase in the density of the immobilized DNA probes, which then helps to monitor more easily the DNA hybridization reaction [19].

In yet another study, Hsu et al., 2014, used the electropolymerization method to incorporate chloro(protoporphyrinato) iron(III) (hemin), polypyrrole (PPy), and silver (Ag) in order to achieve sufficient sensitivity for an environmental dissolved oxygen (DO) sensor. The electropolymerization method provides a strong adhesive bond at the substrate/hemin interface and allows for an increased concentration of hemin. However, due to their poor current collection capacity, electropolymerized films with higher hemin loading do not instead produce proportionally higher current or increased sensitivity. Therefore, co-electropolymerizing hemin and pyrrole to fabricate a sensing electrode for dissolved oxygen sensing applications is one of the better methods for solving this lower sensitivity problem. Thus, this sensor is able to be manufactured at a lower cost and with longer lifespan. In addition, since it is a solid state sensor, it has the potential to be miniaturized and integrated within a micro-fabricated reference electrode to form a complete sensing system at a very low cost [20].

1.2. Electrochemical Sensors

Electrochemical sensors have aroused great interest in providing fast and highly sensitive detection of proteins, which include the antibodies generated during the immune response against infections. Recently, electrochemical sensors have found widespread applications in clinical diagnostics, food safety, food quality, biological analysis, and en-

vironmental monitoring. Electrochemical sensors are sensors that change the effect of an electrochemical reaction of target species on the electrodes into useful signals which demonstrate alterations in potential and conductivity. With the utilization of biofunctionalities in the electrochemical sensor such as recognition and catalysis, these sensors are known as “biosensors” [21]. A typical biosensor is a combination of a transducer and certain biological elements. The biosensor can also be described as an electrochemical, optical, thermal, or piezoelectric biosensor depending on the type of transducer used.

In order to functionalize the biological element during the development of the biosensor, the immobilization step is a crucial step. The most popular biosensor utilizes enzymes as the biological substance with an electrode functioning as a transducer. The enzyme is directly immobilized onto the surface of the electrode, or is immobilized onto the electrode using a suitable matrix. In most cases, there are four strategies for enzyme immobilization that can be considered. These strategies, derived from the chemistry of immobilization, are shown in Figure 2. The first strategy is covalent bonding to the electrode or matrix (Figure 2A). The second is physical adsorption to the electrode or matrix (Figure 2B). The third is entrapment involving the enzyme and the electrode (Figure 2C). The final is affinity, which uses a specific biochemical interaction (Figure 2D). However, these strategies cannot each be considered as the perfect strategy because the optimum biosensor still needs to be selected depending on the specific enzyme and transducer [22].

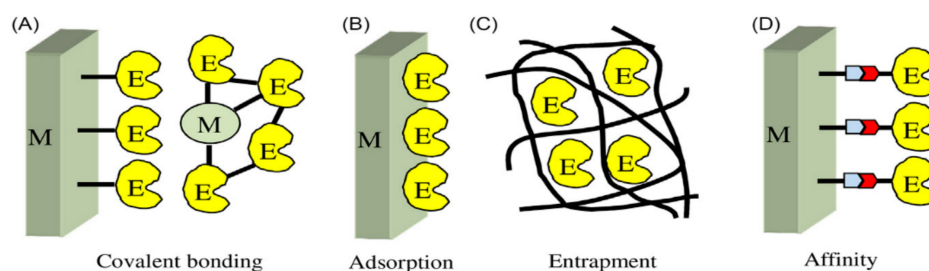


Figure 2. Schematic representation of strategies for enzyme immobilization: Covalent bonding (A); Adsorption (B); Entrapment (C) and Affinity (D). E, enzyme; M, matrix [22]. Reproduced with permission from [H. Muguruma], [Biosensors: Enzyme Immobilization Chemistry]; published by [Elsevier], [2018].

The capture of a target analyte onto a bio or non-bioreceptor immobilized on a CP will generate a measurable analytical signal which is then converted into an electrical signal. The electrical signal can be identified using three main types of sensing modes such as potentiometric (membrane potential change); impedimetric (impedance change); and voltametric or amperometric (change of current for an electrochemical reaction with the applied voltage in the former, or with time at a fixed applied potential in the latter) [23]. It is desirable to strategize the development of an electrochemical sensor in order to provide low detection limits, high selectivity, and utilize a limited amount of indicator species. The impedimetric mode measures the targeted analyte through the output of an electrical impedance signal that is proportional to the analyte activity [9,24]; whereas in the voltametric mode, data about an analyte are obtained by measuring the current while applying a working electrode potential. The electrochemical reaction on the electrode surface and the electrode/electrolyte interface layer produces the final current [25]. The voltametric strategies include linear sweep voltammetry (LSV), cyclic voltammetry (CV), differential pulse voltammetry (DPV), and square wave voltammetry (SWV). These strategies provide a detailed measure with a broad range of effectiveness and a low detection limit. Meanwhile, in the amperometric mode, a consistent potential is connected to the working electrode, resulting in a current over time measurement. The difference between the amperometric and voltametric modes is the use of a potential step instead of a potential sweep. Using the amperometric mode will provide more selectivity and sensitivity since the reduction or oxidation potential utilized in the determination is normal for the analyte sample [26].

In this review, the discussion of sensing modes for the electrochemical sensor will be focused on impedimetric and voltametric modes. It will be start with an introduction followed by a description in detail, then the practical impacts of these modes on the electrochemical sensors will be discussed. We aim to present and highlight how these sensing modes can contribute to rationalizing the optimization of PPy based conducting polymers in electrochemical sensor applications.

2. Impedimetric Sensing Mode

In order to describe the response of a PPy based conducting polymer electrochemical sensor towards a low amplitude sinusoidal perturbation as a function of frequency, the impedimetric sensing mode will be used. Impedimetric mode, also known as impedance, is a circuit's ability to measure the resistance towards the flow of an electrical current. To measure the impedance, an electrochemical impedance spectroscopy (EIS) is used with the application of a small sinusoidal potential to the working electrode in an electrochemical cell, while measuring the resulting current response. By varying the excitation frequency, f , of the applied potential over a range of frequencies, one can calculate the complex impedance, i.e., the sum of the system's real and imaginary impedance components as a function of the frequency (i.e., angular frequency ω). The results of the impedance measurement can be graphically demonstrated using the Nyquist (Cole–Cole) and Bode plot for all the applied frequencies with the real part of the impedance Z plotted along the x -axis and imaginary part plotted along y -axis in the latter [27].

2.1. Nyquist Plot

The Nyquist plot is a plot where the imaginary impedance $Z''(\omega)$ is plotted against real impedance $Z'(\omega)$. Generally, the resistance value can directly obtain from Ohm's law as shown in Equation (1), where the resistance is the ratio between voltage, E , and current, I .

$$R = \frac{E}{I} \quad (1)$$

It assumes an ideal resistor. An ideal resistor occurs when it follows the Ohm's law at all voltage and current levels, where the resistance value is independent of frequency and when AC voltage and current signals are in phase with each other while going through the resistor. However, this does not always happen because in reality, circuit behavior is far more complicated. Therefore, in this concept, the impedance element is much more suitable for use rather than simple resistance to explain the changes measured in the circuit. Impedance is a frequency-dependent measurement of the opposition to current flow in an electric circuit. Impedance measurement is performed by applying an AC excitation voltage to an unknown system while measuring the current. The ratio of the excitation voltage to the current gives the complex impedance of the system.

The first step after impedance measurement is done is the graphical representation from the experimental data. The data from the impedance measurement will consist of three main components which are the real and imaginary impedance, and the frequency. These data will then be represented in Cartesian coordinates as shown in Equation (2):

$$Z(i\omega_i) = Z'_i + iZ''_i \quad (2)$$

Or in polar coordinates as shown in Equation (3):

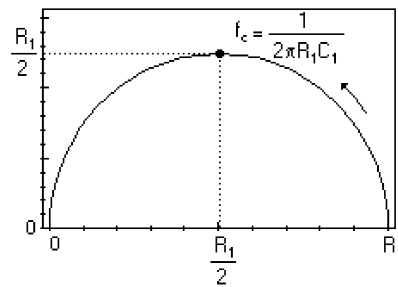
$$Z(i\omega_i) = |Z_i|e^{i\varphi_i} \quad (3)$$

where $|Z_i| = (Z'^2_i + Z''^2_i)^{1/2}$ is the modulus and $\varphi_i = \tan^{-1}(Z''_i / Z'_i)$ is the phase, which corresponds to a given frequency.

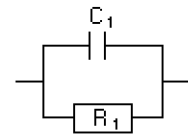
The most common plot for impedance representation is based on Equation (2) which is a Nyquist plot with only one semicircle (Figure 3a). It shows the results from an electrical

equivalent circuit that is depicted in Figure 3b, which consists of a resistor and a capacitor in parallel. The direction of the frequency scanning is from high to low frequencies. At higher frequencies, the capacitor’s impedance will be very low and a major part of the current will flow through the capacitor. With a decrease in the frequency, the capacitor’s impedance increases and a bigger fraction of the current will then flow through the resistor. When most of the current flows through the resistor, the total imaginary resistance Z'' will drop as the real part Z' increases. Sometimes, the plot may consist of several semicircles or only a portion of a semicircle (Figure 3c,e). The different semicircles represent different electrical equivalent circuits and are shown in Figure 3d,f.

Nyquist Diagram (-Im[Z] vs. Re[Z])



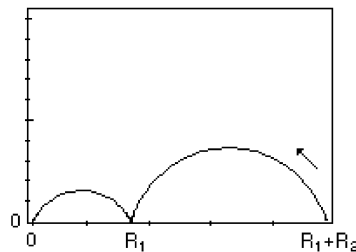
(a)



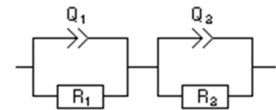
$$Z(f) = \frac{R_1}{1 + j2\pi f R_1 C_1}$$

(b)

Nyquist Diagram (-Im[Z] vs. Re[Z])



(c)

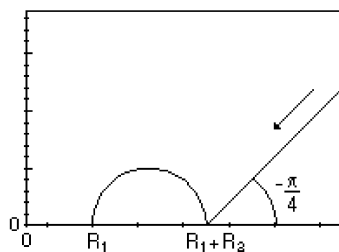


Impedance

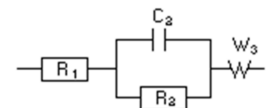
$$Z(f) = \frac{R_1}{R_1 Q_1 (j2\pi f)^{\alpha_1} + 1} + \frac{R_2}{R_2 Q_2 (j2\pi f)^{\alpha_2} + 1}$$

(d)

Nyquist Diagram (-Im[Z] vs. Re[Z])



(e)

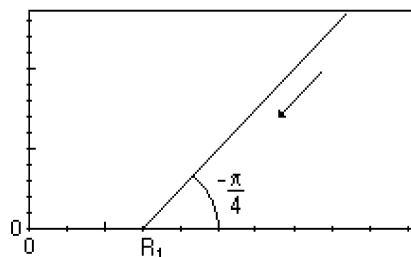


Impedance

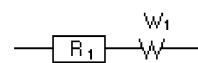
$$Z(f) = R_1 + \frac{R_2}{1 + j2\pi f R_2 C_2} + \frac{\sqrt{2} \sigma_3}{\sqrt{j2\pi f}}$$

(f)

Figure 3. Cont.

Nyquist Diagram ($-\text{Im}[Z]$ vs. $\text{Re}[Z]$)

(g)



$$Z(f) = R_1 + \frac{\sqrt{2} \sigma_1}{\sqrt{i 2 \pi f}}$$

(h)

Figure 3. Nyquist plot with one semicircle and its equivalent circuit (a,b); two semicircles and its equivalent circuit (c,d); one semicircle with spike (45°) and its equivalent circuit (e,f); only spike (45°) and its electrical equivalent circuit (g,h) [28].

The equivalent circuit derived from the plot could then be used to analyze changes or the effects on the electrochemical sensor system that was added or modified. Besides that, the charge transfer resistivity, R_{ct} , also can be obtained from the Nyquist plot. For example, Ramanavicius et al. described an immunosensing system model based on the bovine leukemia virus (BLV) protein (gp51) entrapped within electrochemically synthesized polypyrrole (PPy/gp51). They reported that another element was present in the blood serum sample after it was treated as detected in the fitted equivalent circuit. This was due to the slightly increased measurement of the real part of the impedance spectrum (resistivity increased). It was explained that an additional layer occurred outside the polypyrrole film and proved that the treatment was successful [29]. Devi et al. reported that R_{ct} value was increased with the addition of xanthine oxidase (XOD) in a ZnO-NPs/PPy/Pt electrode, which is due to the immobilization of XOD onto the ZnO-NPs/PPy/Pt surface. It proved that the use of nanocomposites and PPy electrodeposited on the Pt surface electrode as a support for the immobilization of XOD resulted in an improvement of the xanthine biosensor performance with a detection limit of $0.8 \mu\text{M}$ [30]. Meanwhile, Chen et al. used impedance analysis to evaluate the charge separation efficiency of a PPy based photoelectrochemical sensor. There were two semicircles obtained from the impedance curve when Cu_2O was added on top of the ITO electrode. The semicircles known as R_{ct} were then reduced to one and became smaller when fabricated with and without Microcystin-LR and LiClO_4 as template molecules during the electropolymerization process. As R_{ct} become smaller, the charge transfer efficiency become higher [31]. Furthermore, Bao et al. electrodeposited gold nanoparticles/polypyrrole-reduced graphene oxide nanocomposites (Au/PPy-rGO) on top of a bare glass carbon electrode (GCE) in order to produce excellent sensing performance for mRNA-16. The R_{ct} from a small semicircle (bare GCE) was decreased to almost a straight line (after electrodepositing) in the impedance curve results. When it is being further assembled using catalyzed hairpin assembly (CHA), and hybridization chain reaction (HCR), the R_{ct} semicircle was greatly increased, demonstrating the successful CHA and HCR processes and the fact that more negatively charged DNA polymers were linked on the modified electrode [32]. Akshaya and co-workers researched a Palladium–Gold (PdAu) based electrochemical sensor which was developed by electrodepositing PdAu nanoparticles onto a Polypyrrole (PPy) modified carbon fiber paper (CFP) electrode. They found that with the modification of CFP the PPy conducting polymer, the R_{ct} decreased, indicating the conducting nature of PPy. Then, with further electrodeposition of PdAu nanoparticles onto the PPy/CFP, the value of R_{ct} become significantly decreased. This confirmed the formation of a highly conducting electronic pathway at the electrode–electrolyte interface where Pd and Au nanoparticles facilitated electron transfer between the analyte and the electrode [33].

2.2. Bode Plot

Even though the Nyquist plot can give significant information on the resistance of the material used, it has one major shortcoming where it is unable to show the frequency used at the focal data point needed. Each point corresponds to a given frequency which is ω (s^{-1}) or f (Hz), where $\omega = 2\pi f$. Therefore, as an alternative, the data can be represented in a Bode plot by using Equation (3). Generally, the Bode plot provides a more comprehensible description of the electric systems' frequency-dependent behavior than the Nyquist plot, in which frequency values are not clear. In the Bode plot, the data are plotted with log of frequency on the x -axis and both the log of absolute value of the impedance ($|Z|$) and phase-shift (θ) on the y -axis (Figure 4) [34].

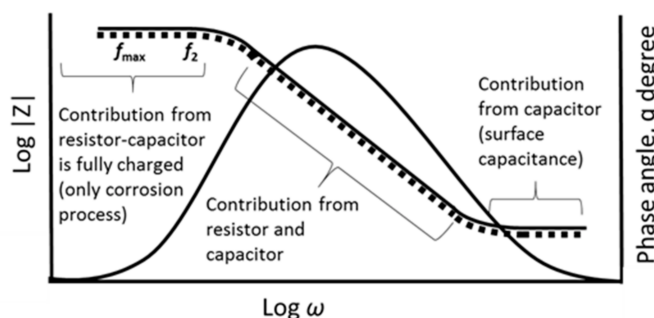


Figure 4. Bode plots of the frequency response (dotted line) and phase angle (solid line) for an electrochemical system.

A typical Bode plot is the same system as shown in Figure 2A. It is simpler to understand as there is only one semicircle that appears on the Nyquist plot. The $\log |Z|$ versus $\log \omega$ curve can be used to determine the values of R_p and R_Ω . At very high and very low frequencies, $|Z|$ becomes independent of frequency. At the highest frequencies, the ohmic resistance controls the impedance and $\log(R_\Omega)$ can be read from the high frequency horizontal level. On the other hand, at the lowest frequencies, $\log(R_p + R_\Omega)$ can be read from the low frequency horizontal portion [35].

Besides that, the Bode plot can also prove the number of semicircles present in the corresponding Nyquist plot. It can be seen from the shapes of the phase angle plots. For example, from the Nyquist plot, a smaller semicircle appears at higher frequencies, followed by second larger semicircle at medium frequencies and a Warburg diffusion effect in low frequencies (Figure 5a). Therefore, to confirm the presence of these two semicircles, the shape from the phase angle graph in the Bode plot will be used (Figure 5b). It can then be seen that the slope is somewhat broadened. Therefore, it proves that there is more than one semicircle present in the Nyquist plot.

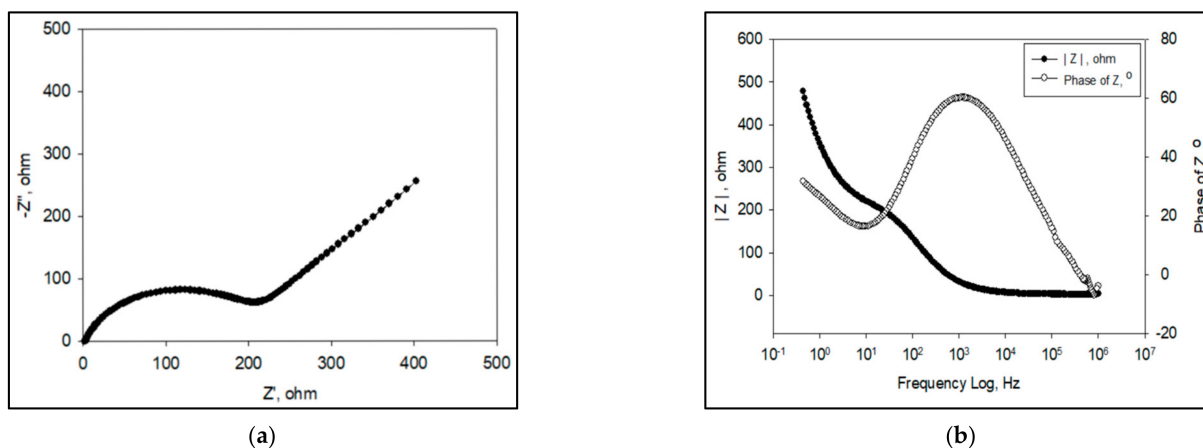


Figure 5. Nyquist plot with two semicircles (a) and Bode plot (b).

Lee et al. has researched a nicotine electrochemical sensor where a copper hexacyanoferrate-polypyrrole (CuHCF-PPy) nanocomposite was deposited directly onto reduced graphene oxide (rGO) by a direct self-assembly technique. From the impedance results, they obtained two semicircles in their Nyquist plot. This was expected and is due to the presence of two layers' of materials comprising of rGO and the metal layer (CuHCF) or metal-polymer layer (CuHCF-PPy) on the electrodes. Therefore, from the Bode plot, two phase angles were observed. The phase angle in the high (f_1) frequency regions was attributed to the R_{ct} which happens across the electrode-electrolyte interface (CuHCF or CuHCF-PPy/solution). Meanwhile, the second phase angle (f_2) was due to the CuHCF or CuHCF-PPy/rGO interface [36]. In research from a different perspective, Ratautaite et al. used Bode plots to evaluate the best frequency for further evaluation of capacity changes as a result of theophylline addition. They found that most sensitive impedance changes were in the frequency range from 10 Hz to 100 Hz. Therefore, in that frequency range, the capacitance changes at certain frequencies were further evaluated [37]. On the other hand, Al-Mokaram et al. used a Bode plot to study the frequency region of R_{ct} of modified electrode nanocomposite films consisting of polypyrrole-chitosan-titanium dioxide (Ppy-CS-TiO₂) in the development of a non-enzymatic glucose biosensor. It was found to collect in the frequency range of 0.01–10,000 Hz. The shifting of peaks toward the low frequency region of 1–0.01 Hz for composite and nanocomposite electrodes indicates the fast electron-transfer behavior of the nanocomposites (Figure 6). A perfect linear portion was observed at lower frequencies for the nanocomposite electrode compared to other electrodes. The results indicated that the Ppy-CS-TiO₂ nanocomposite was successfully designed and it facilitated a diffusion-limited process at the electrode-solution interface [38].

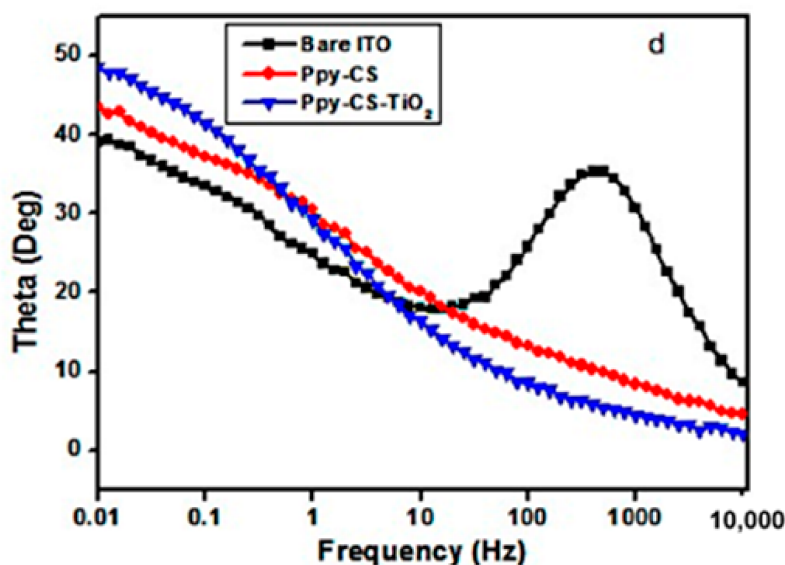


Figure 6. Bode phase plot for 1 mM $K_3(Fe(CN)_6)$ in 0.1 M KCl at a scan rate of 50 mV s⁻¹ vs. (Ag/AgCl) [38].

2.3. Dielectric Constant (ϵ_r)

Impedance measurements analysis can also provide data on the intrinsic dielectric constant and dielectric loss properties of an electrochemical sensor [39]. Dielectric studies are used to understand the mechanism of conduction and dielectric properties that may be valuable in developing a device's performance and in the design of the electronic devices. According to Ramesan and Santhi, who studied conducting polymer composites of polypyrrole (PPy) with different silver doped nickel oxide (Ag-NiO) nanocomposites, the dielectric constant was found to depend on the polarizability of dipoles in the direction of the applied field. From their results, they found that PPy exhibited a lower dielectric constant compared to all of the nanocomposites they studied [40]. Their argument was

supported by Anilkumar et al., who explained that the lower dielectric constant seen in conducting polymers may be attributed to the interfacial polarization of the composite materials. Interfacial polarization mainly arises from the electrical heterogeneities of the composite materials [41]. Strong interfacial interactions between the polymer and nanoparticles reduce the macromolecular chain's cohesive forces, which increases the dielectric constant of the composite. With further loading of the composites (>10 wt%) in the PPy matrix, it was found to decrease the dielectric constant. This is thought to be due to the formation of aggregates within the PPy matrix. They also found that the dielectric loss of composites is higher than that of PPy. The higher dielectric loss observed might be due to the high surface area, surface domain polarization and the quality of the electrical network formation [42]. With further loading of the composite, the dielectric loss was found to decrease. This may be due to the formation of clusters or discrete aggregates in the PPy matrix, which can prevent the migration of charge carriers through the polymer.

2.4. Dielectric Loss ($\tan \delta$)

Dielectric loss is represented by the dissipation factor ($\tan \delta$) which is the amount of dissipated energy or electrical loss by insulating material when a voltage is applied to the material [40]. The dielectric loss of a material is directly related to the electrical conductivity of the corresponding matrix. Usually, from the graph of dielectric loss, it always decreases as the frequencies are increased. This is attributed to the time lagging associated with the orientation of dipoles within the polymer matrix. Ramesan and Santhi also studied dielectric loss in their conducting polymer composite of polypyrrole (PPy) with different silver doped nickel oxide (Ag-NiO) content nanocomposite system and found that the $\tan \delta$ of composites was higher than that of PPy alone. This was similar to their findings in the dielectric constant. Furthermore, when they increased the nanoparticle content, the $\tan \delta$ value of the composite also increased. This may be due to the high surface area, surface domain polarization, and the quality of the electrical network formation. With further loading of nanocomposites (>10 wt%), the $\tan \delta$ value was seen to decrease. This might be caused by the formation of clusters or discrete aggregates in the PPy matrix, which then prevented the migration of charge carriers through the polymer [40]. Besides that, Ramesan and co-workers also worked on different types of nanocomposite and polymer matrices. They studied poly (vinyl cinnamate) (PVCin) with different ratios of zinc oxide (ZnO). Their results showed a similar pattern to the other studies [43].

2.5. Impedimetric PPy Based Electrochemical Sensors and Biosensors

In most EIS studies that involve electrochemical sensors, the use of an electroactive probe/indicator has been employed to evaluate an electrode's signal activity. The advantage of using an electroactive probe is that it can serve as a reference point for impedance studies. For example, Arabali et al. fabricated an amplified tramadol electrochemical sensor based on the surface modification of pencil graphite electrode (PGE) by CuO nanoparticle (CuO-NPs) and polypyrrole (PPy). From the impedance results obtained, it confirmed the modification of PGE with PPy and PPy + CuO-NPs was able to improve the electrical conductivity of the sensor and exhibited a highly sensitive electroanalytical sensor for the determination of tramadol [44]. Furthermore, in humidity sensor applications, impedance analysis is commonly used to study the effect on a conducting polymer composite with various different compositions on the percentage of relative humidity measurement, RH%. Su et al. reported that the addition of PPy-Ag into pristine SnO₂ helped to reduce the impedance resistance, thereby increasing its sensitivity especially at low RH%. The study also proved that the impedance decreased as the amount of PPy-Ag increased. The addition of PPy-Ag helped to increase the mobility of solvated ions inside the system [45]. Meanwhile, Jlassi et al. reported that their findings did not follow this trend. They studied the effect of a combination PPy-Ag with modified halloysite nanoclay (HNT) films on RH% sensitivity at three different wt.% (0.25 wt.%, 0.5 wt.%, and 1 wt.%) amounts. The best finding was achieved using PPy-Ag 0.5 wt.% film due to its hydrophilic behavior. They

found that the impedance decreased as the humidity level increased. This is because the higher the humidity level, the higher the amount of moisture absorbed onto the PPy-Ag film, thereby increasing the conductivity of the film [46].

3. Voltametric Sensing Mode

Voltametric sensing mode is a measurement technique where a current is produced by sweeping the potential applied between a reference electrode and a conducting polymer or a conducting polymer modified electrode over a range that is associated with the redox reaction of the analyte [47,48]. It is also known as voltammetry analysis. There are a number of voltammetry techniques used which are described below.

3.1. Cyclic Voltammetry (CV)

One of the most powerful and popular voltammetry techniques used to investigate the reduction and oxidation processes of molecular species is cyclic voltammetry (CV). CV is an analysis to study electron transfer-initiated chemical reactions, which includes catalysis. Generally, a typical graph with a “duck” shaped curve will be obtained from CV analysis which is called a voltammogram or a cyclic voltammogram, as shown in Figure 7.

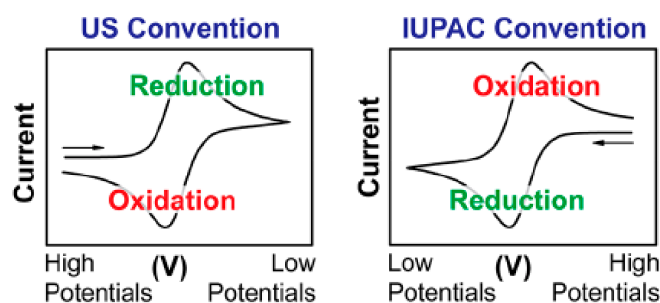


Figure 7. Examples of “duck” shaped cyclic voltammograms [49]. Reproduced with permission from [N. Elgrishi], [A Practical Beginner’s Guide to Cyclic Voltammetry]; published by [ACS Publications], [2017].

From the graph, it can be seen that the x -axis represents the applied potential (E) that is imposed on the system; meanwhile, the y -axis is the resulting current (i) passed, which is the response during the measurement. Some direct information can be obtained from the CV graph, such as that at the potential axis (x -axis), it contains an arrow which indicates the direction of the scanned potential used to record the data. Besides that, it also indicates the beginning and sweep direction of the first segment (or “forward scan”). Sometimes, a crucial parameter also can be found in the graph which is scan rate (v). It indicates that the potential was varied linearly at the speed (scan rate) during the experiment: for example, $v = 100 \text{ mV/s}$ [49].

Figure 8 shows the “duck”-shaped voltammogram of a reversible reduction of 1 mM Fc^+ solution to Fc , at a scan rate of 100 mV/s. As the potential is scanned negatively (cathodically) from point A to point D, (Fc^+) is reduced to Fc and it is steadily depleted near the electrode. Simultaneously, a peak cathodic current ($i_{p,c}$) can be observed at point C [50]. It is dictated by the delivery of additional Fc^+ via diffusion from the bulk solution. The volume of solution at the surface of the electrode containing the reduced Fc , called the diffusion layer, continues to grow throughout the scan. This will then slow down the mass transport of Fc^+ to the electrode. Thus, upon scanning of more negative potentials, the diffusion rate of Fc^+ from the bulk solution to the electrode surface becomes slower, resulting in a decrease in the current as the scan continues ($C \rightarrow D$). When it reaches the switching potential, D, the scan direction is reversed, and the potential is scanned in the positive (anodic) direction. While the concentration of Fc^+ at the electrode surface is depleted, the concentration of Fc at the electrode surface is increased, satisfying the Nernst equation. The Nernst equation (Equation (4)) can be used in order to predict how

a system will respond to a change of concentration of species in solution or a change in the electrode potential. The Fc presented at the electrode surface is oxidized back to Fc⁺ as the applied potential becomes more positive. At points B and E, the concentrations of Fc⁺ and Fc at the electrode surface are equal, following the Nernst equation, $E = E_{1/2}$. This corresponds to the halfway potential between the two observed peaks (C and F) and provides a straightforward way to estimate the $E^{0'}$ for a reversible electron transfer, as noted above. The two peaks are separated due to the diffusion of the analyte to and from the electrode.

$$E = E^0 + \frac{RT}{nF} \ln \frac{(Ox)}{(Red)} = E^0 + 2.3026 \frac{RT}{nF} \log_{10} \frac{(Ox)}{(Red)} \quad (4)$$

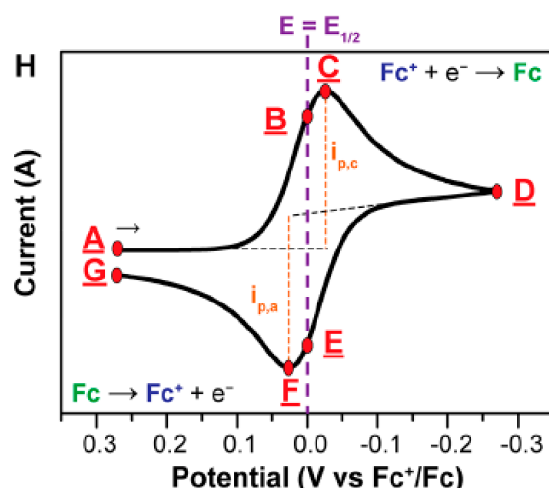


Figure 8. Concentration profiles (mM) for Fc⁺ (blue) and Fc (green) as a function of the distance from the electrode (D, from the electrode surface to the bulk solution, e.g., 0.5 mm) at various points during the voltammogram analysis [49]. (Current flow from A to G.) Reproduced with permission from [N. Elgrishi], [A Practical Beginner's Guide to Cyclic Voltammetry]; published by [ACS Publications], [2017].

Generally, in an electrochemical sensor, cyclic voltammetry is used to study the effect of a conducting polymer's modification towards its current intensity peak. Previously, Kwak et al. reported on the modification of PPy-base with carbon doped polydimethylsiloxane (PPy/CPDMS). Their results showed current peaks during the reduction and oxidation exhibited at a voltage nearby 1.5 V and −1 V, respectively [51]. As the scan rate increases, the currents peak magnitude tends to increase due to the higher scan rate facilitating a thin diffusion layer between the electrolyte and the PPy surface [49]. However, as the scan rate was increased, the voltage at the corresponding current peaks were not identical during the redox reaction. This implied some degree of chemical irreversibility possibly caused by insufficient electron transfer because of the fast scan rate, or the decomposition of the PPy surface [52,53].

Zaabal et.al modified a glassy carbon electrode with polypyrrole (PPy/GCE) to be used as a promising electrode for electrochemical sensing of adefovir (ADV). They reported a weak anodic peak current obtained at 1.559 V for the unmodified electrode. By modifying the GCE with PPy, the anodic peak was shifted to a more negative potential which was 1.484 V accompanied by an enhancement in the peak height of ADV. The higher anodic response of ADV at the PPy/GCE electrode showed that this modified electrode was more sensitive than GCE alone. The enhanced signals and shift of potential peak towards the negative direction indicated that the modified electrode improves electrochemical reactivity of ADV oxidation as compared to bare GCE. This was probably mainly due to the large effective surface area and subtle electronic conductivity of PPy film, which was beneficial to promoting the electron transfer reaction [54].

Besides having a shift in potential axes, the changes in current peak also give important information; for example, in research done by Chen et al. [55] where they prepared a novel polypyrrole/glassy carbon electrode (PPy/GCE) core-zeolitic imidazolate framework-8 (ZIF-8) shell structure composite for quercetin (QR) determination. They found that the current peak of the QR sensor composed of ZIF-8/PPy/GCE was higher than the bare PPy/GCE electrode. It was due to a larger electrocatalytic surface obtained from ZIF-8 and high charge collectability of the host PPy [54]. A similar trend was observed by Hu et al. [56], where they prepared a novel electrochemical sensor based on ion imprinted polypyrrole and reduced graphene oxide (PPy/rGO) composite for trace level determination of cadmium ion (Cd(II)) in water. They found that with the addition of rGO into PPy/GCE, it increased the rate of electron transfer on the electrode surface and amplified the signal response [56].

Furthermore, Yu et al. developed a new electrochemical sensor based on titanium dioxide (TiO₂) and a PPy molecularly imprinted polymer (MIP) nanocomposite for the highly selective detection of p-nonylphenol in food samples. On just the bare GCE, a well-defined reversible redox peak could be observed. When the GCE was modified with PPy and TiO₂, the current intensity peak was obviously enhanced. It suggested that the modification could result in a larger electrochemical surface area, due to the cavities found in the PPy matrix which could accelerate electron transfer of (Fe(CN)₆)^{3-/4-}. After incubation with p-nonylphenol, the MIP absorbed p-nonylphenol molecules and blocked the cavities in the PPy matrix. Thus, the redox peak current intensity decreased as a result of the limitations of electron transfer. In contrast, the electrode modified with PPy and nanoimprinted TiO₂ exhibited a lower current intensity peak compared to PPy with TiO₂ MIP [57].

However, this was found to be different from the findings Ma et al., where they developed an electrochemical biosensor based on sodium alginate-polypyrrole/Au nanoparticles (SA-PPy/AuNPs) nanocomposite for the detection of miRNAs [58]. They reported that the current peak decreased after the modification of bare GCE. The redox peak current of Fe(CN)₆^{4-/3-} slightly decreased due to the poor conductivity of SA and modified hair pin (H1). This could slow down the electron transfer on the surface of the electrode. The GCE/SA-PPy/AuNPs/H1 modified with miRNA-21 and modified hair pin (H2) formed a large number of double helix DNA structures on the surface of the electrode due to the occurrence of the CHA reaction, with a reduction in the redox peak current of Fe(CN)₆^{4-/3-}. Finally, a slight decrease in redox peak current was observed after the copper ion (Cu(II)) complex was inserted onto the double helix DNA structure. This could be attributed to the dissolution of the Cu(II) complex in the mixture of dimethyl sulfoxide (DMSO) and water (H₂O) (volume ratio 7:3). However, the observed poor solubility may have triggered a blockage of the electron transfer between the surface of the electrode and the electrolyte [58].

Besides conducting polymer modifications, the current peak of CV can also be affected by the concentration of a sample [30,59–61]. Zhang et al. designed and constructed an electrochemical ammonia sensor based on Ni foam-supported silver/polypyrrole and platinum nanoparticles electrode (Pt-Ag/PPy-NiF). They studied the effect of ammonia concentration on the oxidation current peak of the PPy/Pt/Ag/NiF electrode and found that its current peak increased when the ammonia concentration increases. This happened because of the strength of the synergistic effect between Ni foam and Pt nanoparticles [59]. Suvina et al. developed a polypyrrole-reduced graphene oxide hydrogel composite electrode for the detection of metal ions. They investigated the effect of metal ion concentration on the PPy-rGO hydrogel electrode and observed that the formation of a multilayer metal ion complex accumulated as a pre-deposited monolayer helped increase the peak current [61]. Meanwhile, Devi et al. prepared a mixture of PPy with synthesized zinc oxide nanoparticles (ZnO-NPs) which were then electropolymerized onto a platinum (Pt) electrode to form a ZnO-NPs-polypyrrole (PPy) composite film. Then, xanthine oxidase (XOD) was immobilized onto the nanocomposite film through physisorption to study the effect

of XOD concentration on the ZnO-NPs/PPy/Pt electrode. They reported that the increases in oxidation current was due to the increased concentration of hydrogen peroxide (H_2O_2) produced during enzymatic reaction [30]. However, it is in contrast to Alagappan et al.'s study, which prepared an electrochemical cholesterol biosensor based on the cholesterol oxidase (ChOx) enzyme immobilized on a gold nanoparticle—functionalized -multiwalled carbon nanotube (MWCNT)—polypyrrole (PPy) nanocomposite modified electrode. They reported that the anodic and cathodic peak currents decreased with an increase in cholesterol concentration. This happened because of an absence of a redox mediator in the system which reduced the electron hopping from the analyte to the enzyme modified electrode [60].

Besides that, the potential difference between the anodic and the cathodic peaks also can be extracted from a cyclic voltammogram. Lo et al. prepared a PPy/CNT/ NH_2 -ITO composite by electropolymerization onto polypyrrole-aminophenyl-modified flexible indium tin oxide (PPy/ NH_2 /ITO) electrodes coated with multi-walled carbon nanotubes (CNTs), in the presence of ethylene glycol-bis(2-aminoethylether)-tetraacetic acid (EGTA) as a chelator. They reported that the potential difference of PPy films deposited onto bare ITO was 430 mV [62]. This was high compared to bare ITO which only exhibited 165 mV [63]. This difference can be linked to the absence of any adhesion between the PPy layer and the bare ITO surface. Meanwhile, in the case of PPy/ NH_2 -ITO, the presence of NH_2 on ITO contributed to an increase in electronic transfers leading to a lower ΔE (181 mV). For PPy/CNT/ NH_2 -ITO, $\Delta E = 321$ mV. The CVs were consistent with those obtained by impedance measurement.

Pineda et al. [64] investigated the effect of polymerization time on the potential and current peak on polypyrrole (PPy) films with a micro tubular structure decorated with gold nanoparticles. The result showed that the anodic current peak from the voltammogram of the PPy film exhibited a cauliflower-like structure, occurring at 0.05 V, and there was found a small cathodic peak at -0.8 V that was led by a small hump at -0.5 V. Furthermore, these anodic and cathodic current peaks were well-defined at ca. 0.28 V and -0.45 V, respectively, as the electropolymerisation time was increased and the tubular structure was formed. This shows that the tubular structure exhibited a better separation between the faradaic and capacitive contributions in a polymeric deposited film [64].

Another aspect that can be studied through cyclic voltammogram is electrocatalytic behavior [65,66]. Xing et al. studied the electrocatalytic behavior of polypyrrole/platinum (PPy/Pt) nanocomposites toward hydrogen peroxide (H_2O_2) reduction. They found that in the absence of H_2O_2 , no reduction peak was observed with bare glassy carbon electrode (GCE), PPy/GCE, and PPy/Pt/GCE. Upon the addition of H_2O_2 , no obvious current from the reduction of H_2O_2 was observed at bare GCE other than a minor increase in the background current. While only a weak reduction peak for H_2O_2 at about -0.28 V was observed on the PPy/GCE electrode, in contrast, on the PPy/Pt/GCE electrode, there was a remarkable reduction peak of H_2O_2 obtained of around -0.2 V. This was even higher than the bare Pt electrode in terms of reduction peak current value, indicating that the PPy/Pt/GCE might provide a better electrocatalytic effect than the bare Pt electrode [65].

The electrocatalytic oxidation of an adenine and guanine mixture at bare and modified PPy/graphene/GCE electrodes were studied by Gao et al. [66]. They reported that there was no oxidation signal observed in the CV curves of the PPy/graphene/GCE electrode due to a blocking effect but there was a high current peak observed with the modified PPy/graphene/GCE electrode. The report also concluded that the overoxidized polypyrrole/graphene/glassy carbon electrode (PPyox/graphene/GCE) electrode had the highest current peak of adenine and guanine oxidation which indicated the highest electrocatalytic activity [66].

3.2. Limit of Detection (LOD)

Voltammetry can be used to obtain quantitative information which is deduced from peak current intensity [48]. Usually, it is used to determine the sensitivity value of the sensor.

Sensitivity, analytical sensitivity, functional sensitivity, lower limit of detection (LOD), etc., are terms used to describe the smallest concentration of a measure that can be measured (detected) with statistical significance employing a given analytical procedure [67]. It is also defined as the minimum input quantity that can be distinguished with more than 99% reliability [68]. *LOD* is also a valuable quantitative measurement usually in the healthcare industry where it can be used as a biomarker in the detection of disease, environmental pollutants such as heavy metals, and other chemical contaminants that are part of the environmental liability in contemporary societies [69]. The value of the *LOD* can be determined through calculation using Equation (5).

The equation to calculate the *LOD* is:

$$LOD = \frac{3 \times SD}{m} \quad (5)$$

where *SD* is the magnitude of the error bar at blank while *m* is the slope of the calibration curve of the blank [69]. Before it can be calculated, a graph of current or current density with different concentrations of the sensing material needs to be plotted (Figure 9a).

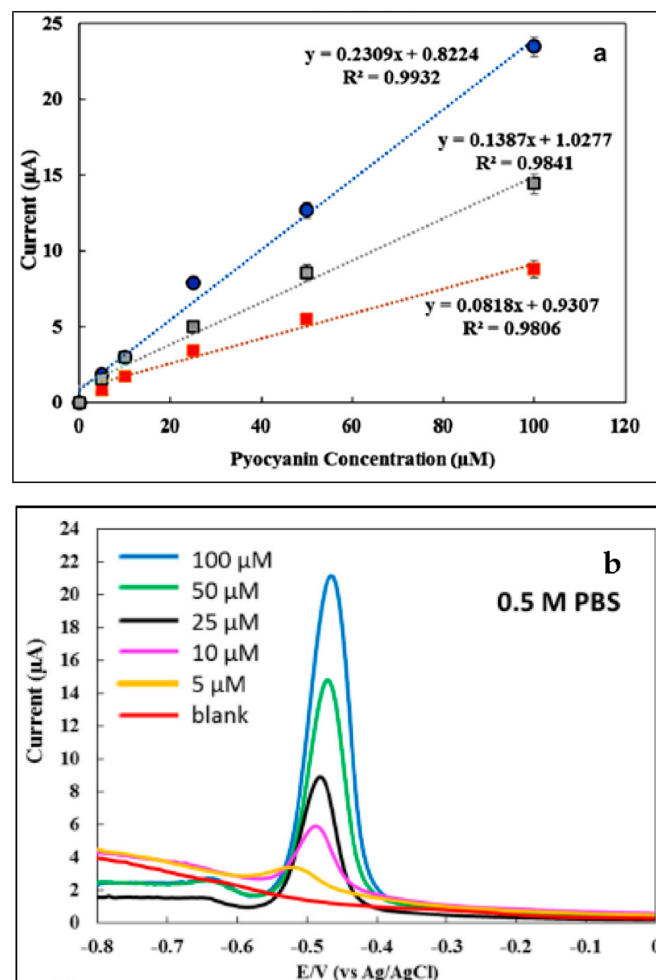


Figure 9. Example graphs of current response with different concentrations of pyocyanin biomarker using a DPV analyzer where the calibration curve for the three different mediums (0.5 M PBS at pH 7.4 (blue), human urine (grey) and human saliva (red)) at the potential range of -0.8 V to 0 V (a) and DPV current response of pyocyanin (5–100 μM) in 0.5 M PBS (b) [70]. Reproduced with permission from [J.I.A.Rashid], [An electrochemical sensor based on gold nanoparticles-functionalized reduced graphene oxide screen printed electrode for the detection of pyocyanin biomarker in *Pseudomonas aeruginosa* infection]; published by [Elsevier], [2020].

The current peak (i_p) value can be obtained either from the peak of a cyclic voltammogram (CV), differential pulse voltammogram (DPV), or square wave voltammogram (SWV). Most researchers use DPV and SWV to determine the current peak (Figure 9b). This is because of the high sensitivity of the technique compared to CV. In general, CV can provide essential information, such as the reversibility process and types of redox processes present in an analysis (matrix, analyte, and electrode); however, DPV and SWV are used for quantitative determinations [71].

3.3. Differential Pulse Voltammogram (DPV)

DPV is a technique that involves applying amplitude potential pulses on a linear ramp potential. In DPV, a base potential value is chosen at which there is no faradaic reaction and is then applied to the electrode. The base potential is increased between pulses with equal increments. The current is immediately measured before the pulse application and at the end of the pulse, and the difference between them is recorded (Figure 10). DPV is similar to the first derivative of a linear voltammogram in which the formation of a peak is observed for a given redox process. In the linear sweep technique, it has a shape similar to a wave, and the first derivative originates a peak.

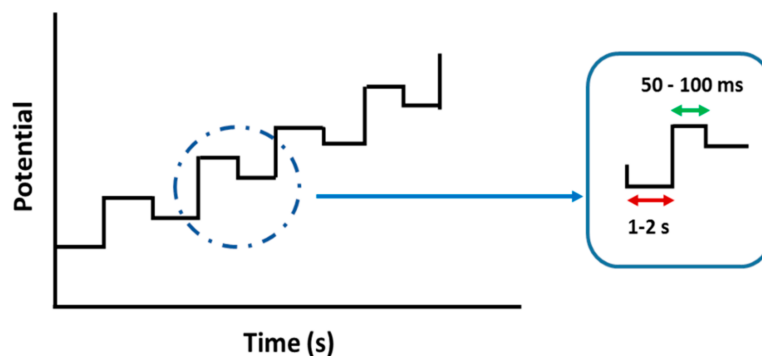


Figure 10. Diagram of the application of pulses in differential pulse voltammetry (DPV).

As in polarography (dropping mercury electrode), the qualitative information of an analyte is given by its half-wave potential ($E_{1/2}$), which corresponds to the potential at half the wave height. Similarly, in DPV, the peak potential, E_p , can be approximately identified through $E_{1/2}$. Increasing the irreversibility, E_p deviates from $E_{1/2}$ as the base of the peak widens and its height decreases. The DPV is therefore a graph of differences between measured currents and applied potentials as shown in Figure 9b [69,72].

3.4. Square Wave Voltammogram (SWV)

Meanwhile, SWV is the fastest and the most sensitive pulse voltammetry technique. The detection limits can be compared with those of chromatographic and spectroscopic techniques. In addition, the analysis of the characteristic parameters of this technique also enables the evaluation of the kinetics and mechanism of the electrode process under study [71,73]. According to Marie et al., the lower limit of detection value means the lowest concentration of glucose (analyte) that can be detected by the device [74].

Zhang et al. constructed an aqueous ammonia sensor using a low cost, high sensitivity, and great stability construct based on Ni foam-supported silver/polypyrrole and platinum nanoparticles electrode (Pt-Ag/PPy-NiF). They found that the ammonia sensor showed a sensitivity of $0.089 \text{ mA } \mu\text{M}^{-1}$ with a detection limit of 37 nM and a wide linear range, as well as possessing a good anti-interference capability against many common ions found in water. The Pt-Ag/PPy-NiF electrode possessed a lower detection limit and higher sensitivity compared to most electrochemical aqueous ammonia sensors. Its excellent performance can be mainly attributed to the large specific surface area of the electrode and great electrocatalytic ability of Pt nanoparticles [59].

Salunke et al. prepared a sensor device by electrodepositing gold nanoparticles onto a single PPy nanowire for arsenic detection. They found that the sensitivity of Au-NPs decorated PPy-NW towards arsenic (for two set of as conc. range) was 0.22 and 4.38 μM^{-1} with a good detection limit of 0.32 μM . Their result was better in respect of sensitivity and LOD, and this could be due to the change in sensor dimensions where they used nanowire as a base material and the gold nanoparticles as the sensing material. This led to the finding of a high surface area as being a dimension factor for the enhancement of sensor sensitivity with rapid detection and accuracy [75].

In other work done by Zaabal et al., they studied a polypyrrole modified glassy carbon electrode (PPy/GCE) for the electrochemical sensing of adefovir (ADV). ADV is a broad-spectrum antiviral agent whose action is as a DNA polymerase inhibitor. The detection limit of ADV obtained was 3.10 nM. Moreover, they also determined ADV in human serum and urine and found that the detection limit was 0.06 μM and 0.04 μM , respectively. Their detection limit value was much lower compared to the findings in other research works [76,77]. This showed that PPy/GCE can be an effective alternative sensor for the electrochemical determination of ADV in commercial pharmaceutical dosage forms and biological fluids.

3.5. PPy Based Voltammetric Sensor

In order to develop sensitive detection instruments, different signal amplification strategies also can be utilized to improve the sensitivity of the sensors used. Ma et al. designed an ultrasensitive and specific electrochemical biosensor for the determination of miRNAs based on SA-PPy/AuNPs. It was analyzed using the SWV technique with a dual signal amplification strategy involving the catalytic hairpin assembly (CHA) reaction and $\text{Cu}^{2+}/\text{Fe}^{3+}$ catalytic reaction [58]. They found that, with the usage of this dual signal amplification strategy and a sensitive analyzer technique, which was SWV, the LOD value was significantly improved and could be as low as 0.34 fM compared to other research work [78–81]. Table 1 shows the comparison of different methods and signal amplification strategies with miRNA-21 as the target. The CHA reaction was triggered and numerous double helix-DNA were formed in the presence of the target miRNA. Furthermore, the intercalated planar Cu (II) complex could bind with the double-helix DNA, which was employed as a signal amplification molecule in the presence of Fe^{3+} . After the dual signal amplification, the reduction of the Cu (II) complex was recorded to represent miRNA levels.

Table 1. Comparison of different methods and signal amplification strategies with miRNA-21 as the target.

Detection Method	Signal Amplification Strategy	LOD Value	References
Fluorescence	Ligase mediated amplification	314 fM	Chan et al. [80]
DPV	$\text{Fe}(\text{CN})_6^{3+}$	10 fM	Low et al. [79]
Chemiluminescence	Cascade enzyme catalytic reaction	1 fM	He et al. [81]
DPV	CHA reaction and RCA	13.5 fM	Wang et al. [78]
SWV	CHA reaction and $\text{Cu}^{2+}/\text{Fe}^{3+}$ catalytic reaction	0.34 fM	Ma et al. [58]

Table 2 summarizes the electrochemical sensing modes of PPy based electrochemical sensors reviewed in this paper with their possible applications.

Table 2. Summary of electrochemical sensing modes of PPy-based electrochemical sensors with their applications.

Material	Modification/Improvement	Electrochemical Sensing Mode	Application	References
- PPy	SnO ₂ Ag-SnO ₂	Impedimetric	Humidity sensor	Su et al. 2020 [45]
PPy PPy PPy PPy	Ag (0.5 wt.%) HNT-DMA ITO NH ₂ -ITO CNT-NH ₂ -ITO	Impedimetric Impedimetric Voltammetric	Humidity sensor Lead ion detector	Jlassi et al. 2020 [46] Lo et al. 2020 [62]
PPy	MIP(UA)	Impedimetric	Electrochemical quartz crystal microbalance-based sensor	Plausinaitis et al. 2020 [82]
PPy	GCE GCE-SA-AuNPs	Impedimetric Voltammetric	Dectector for miRNA-21	Ma et al. 2020 [58]
PPy PPy	CFP CFP CFP-PdAu	Impedimetric Voltammetric	MMA detector	Akshaya et al. 2020 [31]
PPy	GCE	Voltammetric	Electrochemical sensing of Adefovir	Zaabal et al. 2020 [54]
PPy	Pt-Ag-NiF	Voltammetric	Aqueous ammonia sensor	Zhang et al. 2020 [59]
PPy	Carbon doped polydimethylsiloxane	Impedimetric Voltammetric	Resistive sensor	Kwak et al. 2019 [51]
PPy PPy PPy PPy	GCE TiO ₂ -MIP-Nafion-GCE TiO ₂ -MIP-Nafion-GCE in 0.1mM p-nonylphenol NP-TiO ₂ -MIP-Nafion-GCE TiO ₂ NIP/Nafion/GCE	Impedimetric Voltammetric	Food sensor: p-nonylphenol analysis (milk powder)	Yu et al. 2019 [57]
PPy PPy	CuHCF CuHCF rGO rGO-CuHCF rGO-CuHCF	Impedimetric voltammetric	Nicotine detector	Lee et al. 2019 [36]
PPy	SS-Au	Impedimetric voltammetric	Detection of hydroxylamine, nitrite and their mixture	Pineda et al. 2018 [64]
PPy PPy	GCE ZIF-8 nanoparticle ZIF-8 nanoparticle	Impedimetric voltammetric	Quercetin detector	Chen et al. 2019 [55]
PPy	rGO-GCE	Voltammetric	Cadmium detector	Hu et al. 2019 [56]
PPy	GCE Au-rGO-GCE	Impedimetric Voltammetric	Biosensor: microRNA detector	Bao et al. 2019 [32]
PPy	MCM-41 GCE	Impedimetric	Humidity sensor	Qi et al. 2018 [83]
PPy PPy PPy	GCE GCE- Au- <i>f</i> -MWCNT Au- <i>f</i> -MWCNT-ChOx-GCE	Impedimetric Voltammetric	Biosensor for cholesterol detection	Alagappan et al. 2018 [60]
PPy PPy PPy	Cu ₂ O-ITO NIP-Cu ₂ O-ITO MIP-Cu ₂ O-ITO	Impedimetric	Imprinted PEC sensor	Chen et al. 2018 [31]
PPy	rGO hydrogel	Voltammetric	Metal ions sensor	Suvina et al. 2018 [61]
Ppy	Au-NPs-NW	Voltammetric	Arsenic detector	Salunke et al. 2017 [75]
PPy PPy	Pt nanocomposite Pt-GCE	Voltammetric	Non-enzymatic electrochemical sensor	Xing et al. 2015 [65]
PPyox	Gr nanocomposite-GCE	Voltammetric	DNA & RNA sensor: detection of adenine and guanine	Gao et al. 2014 [66]
PPy PPy PPy	Pt Pt ZnO-NPs-Pt XOD-ZnO-NPs-Pt	Impedimetric Voltammetric	Xanthine biosensor	Devi et al. 2011 [30]

4. Conclusions

This review presents an overview of the two main electrochemical sensing modes used with electrochemical sensors based on PPy conducting polymers and outlines the significant advances in this field. In this review, the PPy heterocyclic-based conducting polymer was chosen due to its good environmental stability, high electronic conductivity, and biocompatibility. Conducting polymers are considered good sensitive materials for the development of selective, specific, and stable sensing devices. However, having PPy alone as the conducting polymer might not give the best results for an electrochemical sensor or biosensor application. Therefore, modification of the conducting polymer is the way to enhance its properties. To get an in-depth overview of how the modification can improve electrochemical and biosensors, the two main electrochemical techniques, impedimetric and voltametric, should be utilized. From this review, it can be seen that these two techniques play an important role in order to determine the resistivity, reactivity, and sensitivity of the PPy based conducting polymers for use in electrochemical sensors and biosensors. Besides that, they can also help the understanding of the reactivity that occurs when modification of the PPy conducting polymer has been done.

Author Contributions: Conceptualization, N.A.D., J.I.A.R., M.M. and S.A.M.N.; writing—original draft preparation, N.A.D., J.I.A.R., M.M. and S.A.M.N.; writing—review and editing, N.A.D., J.I.A.R., M.M., V.F.K. and S.A.M.N.; visualization, N.A.D., J.I.A.R., M.M. and S.A.M.N.; supervision, S.A.M.N.; funding acquisition, V.F.K., K.K.O., N.A.M.K., W.M.Z.W.Y. and S.A.M.N. All authors have read and agreed to the published version of the manuscript.

Funding: This research received no external funding.

Institutional Review Board Statement: Not applicable.

Informed Consent Statement: Not applicable.

Acknowledgments: The authors are grateful to the Ministry of Education Malaysia, Development Fund F0020 for funding via UPNM/2018/CHEMDEF/ST/5.

Conflicts of Interest: The authors declare no conflict of interest.

References

1. Tsakova, V.; Seeber, R. Conducting polymers in electrochemical sensing: Factors influencing the electroanalytical signal. *Anal. Bioanal. Chem.* **2016**, *408*, 7231–7241. [[CrossRef](#)]
2. Wegner, G. Polymers with Metal-Like Conductivity—A Review of their Synthesis, Structure and Properties. *Angew. Chem. Int. Ed. Engl.* **1981**, *20*, 361–381. [[CrossRef](#)]
3. Bashir, S.; Ramesh, S.; Ramesh, K.; Numan, A.; Iqbal, J. *Conducting Polymer Composites in Electrochemical Sensors*; Central West Publishing: Orange, Australia, 2018.
4. Wang, X.; Gu, X.; Yuan, C.; Chen, S.; Zhang, P.; Zhang, T.; Yao, J.; Chen, F.; Chen, G. Evaluation of biocompatibility of polypyrrole in vitro and in vivo. *J. Biomed. Mater. Res.* **2004**, *68*, 411–422. [[CrossRef](#)]
5. Ansari, R. Polypyrrole conducting electroactive polymers: Synthesis and stability studies. *J. Chem.* **2006**, *3*, 186–201. [[CrossRef](#)]
6. Gupta, V.K.; Yola, M.L.; Özalpın, N.; Atar, N.; Üstündağ, Z.; Uzun, L. Molecular imprinted polypyrrole modified glassy carbon electrode for the determination of tobramycin. *Electrochim. Acta* **2013**, *112*, 37–43. [[CrossRef](#)]
7. Zaabal, M.; Douliche, M.; Bakirhan, N.K.; Kaddour, S.; Saidat, B.; Ozkan, S.A. A facile strategy for construction of sensor for detection of ondansetron and investigation of its redox behavior and thermodynamic parameters. *Electroanalysis* **2019**, *31*, 1279–1290. [[CrossRef](#)]
8. Apetrei, C. Novel method based on polypyrrole-modified sensors and emulsions for the evaluation of bitterness in extra virgin olive oils. *Food Res. Int.* **2012**, *48*, 673–680. [[CrossRef](#)]
9. Ramanaviciene, A.; Ramanavicius, A. Pulsed amperometric detection of DNA with an ssDNA/polypyrrole-modified electrode. *Anal. Bioanal. Chem.* **2004**, *379*, 287–293. [[CrossRef](#)]
10. Viau, L.; Hihn, J.; Lakard, S.; Moutarlier, V.; Flaud, V.; Lakard, B. Full characterization of polypyrrole thin films electrosynthesized in room temperature ionic liquids, water or acetonitrile. *Electrochim. Acta* **2014**, *137*, 298–310. [[CrossRef](#)]
11. Li, M.; Zhu, H.; Mao, X.; Xiao, W.; Wang, D. Electropolymerization of polypyrrole at the three-phase interline: Influence of polymerization conditions. *Electrochim. Acta* **2013**, *92*, 108–116. [[CrossRef](#)]
12. Nautiyal, A.; Qiao, M.; Cook, J.E.; Zhang, X.; Huang, T.-S. High performance polypyrrole coating for corrosion protection and biocidal applications. *Appl. Surf. Sci.* **2018**, *427*, 922–930. [[CrossRef](#)]

13. Wang, J.; Chen, J.; Wang, C.; Zhou, D.; Too, C.O.; Wallace, G.G. Electrochemical synthesis of polypyrrole films using stainless steel mesh as substrate for battery application. *Synth. Met.* **2005**, *153*, 117–120. [[CrossRef](#)]
14. Dubal, D.; Patil, S.; Jagadale, A.; Lokhande, C. Two step novel chemical synthesis of polypyrrole nanoplates for supercapacitor application. *J. Alloy. Compd.* **2011**, *509*, 8183–8188. [[CrossRef](#)]
15. Yusoff, N. Graphene–Polymer Modified Electrochemical Sensors. In *Graphene-Based Electrochemical Sensors for Biomolecules*; Elsevier B.V.: Amsterdam, The Netherlands, 2019; pp. 155–186.
16. Hosseini, S.H.; Entezami, A.A. Conducting polymer blends of polypyrrole with polyvinyl acetate, polystyrene, and polyvinyl chloride based toxic gas sensors. *J. Appl. Polym. Sci.* **2003**, *90*, 49–62. [[CrossRef](#)]
17. Song, Y.; Bian, C.; Hu, J.; Li, Y.; Tong, J.; Sun, J.; Gao, G.; Xia, S. Porous polypyrrole/graphene oxide functionalized with carboxyl composite for electrochemical sensor of trace cadmium (II). *J. Electrochem. Soc.* **2019**, *166*, B95. [[CrossRef](#)]
18. Hassanein, A.; Salahuddin, N.; Matsuda, A.; Kawamura, G.; Elfiky, M. Fabrication of biosensor based on Chitosan-ZnO/Polypyrrole nanocomposite modified carbon paste electrode for electroanalytical application. *Mater. Sci. Eng. C* **2017**, *80*, 494–501. [[CrossRef](#)]
19. Tlili, C.; Korri-Youssoufi, H.; Ponsonnet, L.; Martelet, C.; Jaffrezic-Renault, N.J. Electrochemical impedance probing of DNA hybridisation on oligonucleotide-functionalised polypyrrole. *Talanta* **2005**, *68*, 131–137. [[CrossRef](#)]
20. Hsu, L.; Selvaganapathy, P.R.; Brash, J.; Fang, Q.; Xu, C.-Q.; Deen, M.J.; Chen, H. Development of a low-cost hemin-based dissolved oxygen sensor with anti-biofouling coating for water monitoring. *IEEE Sens. J.* **2014**, *14*, 3400–3407. [[CrossRef](#)]
21. Turner, A.; Karube, I.; Wilson, G.S. *Biosensors: Fundamentals and Applications*; Oxford University Press: New York, NY, USA, 1987.
22. Muguruma, H. Biosensors: Enzyme immobilization chemistry. In *Encyclopedia of Interfacial Chemistry: Surface Science and Electrochemistry*; Elsevier: Amsterdam, The Netherlands, 2018; pp. 64–71.
23. Antuña-Jiménez, D.; Díaz-Díaz, G.; Blanco-López, M.C.; Lobo-Castañón, M.J.; Miranda-Ordieres, A.J.; Tuñón-Blanco, P. Chapter 1—Molecularly Imprinted Electrochemical Sensors: Past, Present, and Future. In *Molecularly Imprinted Sensors*; Li, S., Ge, Y., Piletsky, S.A., Lunec, J., Eds.; Elsevier: Amsterdam, The Netherlands, 2012; pp. 1–34.
24. Yang, L.; Guiseppi-Elie, A. Impedimetric Biosensors for Nano- and Microfluidics. In *Encyclopedia of Microfluidics and Nanofluidics*; Li, D., Ed.; Springer US: Boston, MA, USA, 2008; pp. 811–823.
25. Wang, B.; Wang, L.; Li, X.; Liu, Y.; Zhang, Z.; Hedrick, E.; Safe, S.; Qiu, J.; Lu, G.; Wang, S. Template-free fabrication of vertically-aligned polymer nanowire array on the flat-end tip for quantifying the single living cancer cells and nanosurface interaction. *Manuf. Lett.* **2018**, *16*, 27–31. [[CrossRef](#)]
26. Wang, J.; Musameh, M.; Lin, Y. Solubilization of carbon nanotubes by Nafion toward the preparation of amperometric biosensors. *J. Am. Chem. Soc.* **2003**, *125*, 2408–2409. [[CrossRef](#)]
27. Zia, A.I.; Syaifudin, A.M.; Mukhopadhyay, S.; Yu, P.; Al-Bahadly, I.H.; Gooneratne, C.P.; Kosel, J.; Liao, T.-S. Electrochemical Impedance Spectroscopy Based MEMS Sensors for Phthalates Detection in Water and Juices. *J. Phys. Conf. Ser. IOP Publ.* **2013**, *439*, 012026. [[CrossRef](#)]
28. Instruments, B.S. *EC-Lab Software V.10.40*; Bio-Logic-Science Instruments: Seyssinet-Pariset, France, 2007.
29. Ramanavicius, A.; Finkelsteinas, A.; Cesiulis, H.; Ramanaviciene, A. Electrochemical impedance spectroscopy of polypyrrole based electrochemical immunosensor. *Bioelectrochemistry* **2010**, *79*, 11–16. [[CrossRef](#)] [[PubMed](#)]
30. Devi, R.; Thakur, M.; Pundir, C. Construction and application of an amperometric xanthine biosensor based on zinc oxide nanoparticles–polypyrrole composite film. *Biosens. Bioelectron.* **2011**, *26*, 3420–3426. [[CrossRef](#)]
31. Chen, J.; Gao, P.; Wang, H.; Han, L.; Zhang, Y.; Wang, P.; Jia, N. A PPy/Cu₂O molecularly imprinted composite film-based visible light-responsive photoelectrochemical sensor for microcystin-LR. *J. Mater. Chem. C* **2018**, *6*, 3937–3944. [[CrossRef](#)]
32. Bao, J.; Hou, C.; Zhao, Y.; Geng, X.; Samalo, M.; Yang, H.; Bian, M.; Huo, D. An enzyme-free sensitive electrochemical microRNA-16 biosensor by applying a multiple signal amplification strategy based on Au/PPy-rGO nanocomposite as a substrate. *Talanta* **2019**, *196*, 329–336. [[CrossRef](#)]
33. Akshaya, K.; Anitha, V.; Nidhin, M.; Sudhakar, Y.; Louis, G. Electrochemical sensing of vitamin B12 deficiency marker methylmalonic acid using PdAu-PPy tailored carbon fiber paper electrode. *Talanta* **2020**, *217*, 121028. [[CrossRef](#)]
34. Silverman, D.C. *Tutorial on Cyclic Potentiodynamic Polarization Technique*; United States: Washington, DC, USA, 1998.
35. Poursaeed, A. Corrosion measurement and evaluation techniques of steel in concrete structures. In *Corrosion of Steel in Concrete Structures*; Woodhead Publishing: Southston, UK, 2016; pp. 169–191.
36. Lee, P.K.; Woi, P.M. Direct self-assembly of CuHCF-PPy nanocomposites on rGO for amperometric nicotine sensing at high concentration range. *J. Electroanal. Chem.* **2019**, *837*, 67–75. [[CrossRef](#)]
37. Ratautaite, V.; Janssens, S.D.; Haenen, K.; Nesládek, M.; Ramanaviciene, A.; Baleviciute, I.; Ramanavicius, A. Molecularly imprinted polypyrrole based impedimetric sensor for theophylline determination. *Electrochim. Acta* **2014**, *130*, 361–367. [[CrossRef](#)]
38. Al-Mokaram, A.; Amir, M.A.; Yahya, R.; Abdi, M.M.; Mahmud, H.N.M.E. The development of non-enzymatic glucose biosensors based on electrochemically prepared polypyrrole–chitosan–titanium dioxide nanocomposite films. *Nanomaterials* **2017**, *7*, 129. [[CrossRef](#)] [[PubMed](#)]
39. Sun, T.; Morgan, H. Impedance Measurements of Cells. In *Encyclopedia of Microfluidics and Nanofluidics*; Li, D., Ed.; Springer US: Boston, MA, USA, 2013; pp. 1–4.

40. Ramesan, M.; Santhi, V. Synthesis, characterization, conductivity and sensor application study of polypyrrole/silver doped nickel oxide nanocomposites. *Compos. Interfaces* **2018**, *25*, 725–741. [[CrossRef](#)]
41. Anilkumar, T.; Ramesan, M. Synthesis and Electrical Conductivity Studies of Metal Chloro and Nitroxide Group Containing Styrene Butadiene Rubber. *AIP Conf. Proc. Am. Inst. Phys.* **2014**, *1620*, 28–34.
42. Ramesan, M.T.; George, A.; Jayakrishnan, P.; Kalaprasad, G. Role of pumice particles in the thermal, electrical and mechanical properties of poly (vinyl alcohol)/poly (vinyl pyrrolidone) composites. *J. Therm. Anal. Calorim.* **2016**, *126*, 511–519. [[CrossRef](#)]
43. Ramesan, M.; Nidhisha, V.; Jayakrishnan, P. Synthesis, characterization and conducting properties of novel poly (vinyl cinnamate)/zinc oxide nanocomposites via in situ polymerization. *Mater. Sci. Semicond. Process.* **2017**, *63*, 253–260. [[CrossRef](#)]
44. Arabali, V.; Malekmohammadi, S.; Karimi, F. Surface amplification of pencil graphite electrode using CuO nanoparticle/polypyrrole nanocomposite; A powerful electrochemical strategy for determination of tramadol. *Microchem. J.* **2020**, *158*, 105179. [[CrossRef](#)]
45. Su, P.-G.; Lu, P.-H. Electrical and Humidity-Sensing Properties of Impedance-Type Humidity Sensors that Were Made of Ag Microwires/PPy/SnO₂ Ternary Composites. *Chemosensors* **2020**, *8*, 92. [[CrossRef](#)]
46. Jlassi, K.; Mallick, S.; Mutahir, H.; Ahmad, Z.; Touati, F. Synthesis of In Situ Photoinduced Halloysite-Polypyrrole@ Silver Nanocomposite for the Potential Application in Humidity Sensors. *Nanomaterials* **2020**, *10*, 1426. [[CrossRef](#)] [[PubMed](#)]
47. Kissinger, P.; Heineman, W.R. *Laboratory Techniques in Electroanalytical Chemistry, Revised and Expanded*; CRC Press: New York, NY, USA, 2018.
48. Lakard, B. Electrochemical Biosensors Based on Conducting Polymers: A Review. *Appl. Sci.* **2020**, *10*, 6614. [[CrossRef](#)]
49. Elgrishi, N.; Rountree, K.J.; McCarthy, B.D.; Rountree, E.S.; Eisenhart, T.T.; Dempsey, J.L. A practical beginner's guide to cyclic voltammetry. *J. Chem. Educ.* **2018**, *95*, 197–206. [[CrossRef](#)]
50. Compton, R.G.; Banks, C.E. *Understanding Voltammetry*; World Scientific: Hackensack, NJ, USA; London, UK, 2018.
51. Kwak, B.; Bae, J. Integrated Design and Fabrication of a Conductive PDMS Sensor and Polypyrrole Actuator Composite. *IEEE Robot. Autom. Lett.* **2020**, *5*, 3753–3760. [[CrossRef](#)]
52. Espinoza, E.M.; Clark, J.A.; Soliman, J.; Derr, J.B.; Morales, M.; Vullev, V.I. Practical aspects of cyclic voltammetry: How to estimate reduction potentials when irreversibility prevails. *J. Electrochem. Soc.* **2019**, *166*, H3175. [[CrossRef](#)]
53. Brownson, D.A.; Banks, C.E. *The Handbook of Graphene Electrochemistry*; Springer: London, UK, 2014.
54. Zaabal, M.; Bakirhan, N.K.; Douliche, M.; Kaddour, S.; Saidat, B.; Ozkan, S.A. A New Approach on Sensitive Assay of Adefovir in Pharmaceutical and Biological Fluid Samples Using Polypyrrole Modified Glassy Carbon Electrode. *Sens. Actuators B Chem.* **2020**, *323*, 128657. [[CrossRef](#)]
55. Chen, Y.; Huang, W.; Chen, K.; Zhang, T.; Wang, Y.; Wang, J. Facile fabrication of electrochemical sensor based on novel core-shell PPy@ ZIF-8 structures: Enhanced charge collection for quercetin in human plasma samples. *Sens. Actuators B Chem.* **2019**, *290*, 434–442. [[CrossRef](#)]
56. Hu, S.; Gao, G.; Liu, Y.; Hu, J.; Song, Y.; Zou, X. An Electrochemical Sensor Based on ion Imprinted PPy/rGO Composite for Cd (II) Determination in Water. *Int. J. Electrochem. Sci.* **2019**, *14*, 11714–11730. [[CrossRef](#)]
57. Yu, M.; Wu, L.; Miao, J.; Wei, W.; Liu, A.; Liu, S. Titanium dioxide and polypyrrole molecularly imprinted polymer nanocomposites based electrochemical sensor for highly selective detection of p-nonylphenol. *Anal. Chim. Acta* **2019**, *1080*, 84–94. [[CrossRef](#)] [[PubMed](#)]
58. Ma, X.; Qian, K.; Ejeromedoghene, O.; Kandawa-Schulz, M.; Wang, Y. Electrochemical detection of microRNA based on SA-PPy/AuNPs nanocomposite with the signal amplification through catalytic hairpin assembly reaction and the spontaneous catalytic reaction of Fe³⁺/Cu²⁺. *Electrochim. Acta* **2020**, *362*, 137168. [[CrossRef](#)]
59. Zhang, L.; Liu, J.; Peng, X.; Cui, Q.; He, D.; Zhao, C.; Suo, H. Fabrication of a Ni foam-supported platinum nanoparticles-silver/polypyrrole electrode for aqueous ammonia sensing. *Synth. Met.* **2020**, *259*, 116257. [[CrossRef](#)]
60. Alagappan, M.; Immanuel, S.; Sivasubramanian, R.; Kandaswamy, A. Development of cholesterol biosensor using Au nanoparticles decorated f-MWCNT covered with polypyrrole network. *Arab. J. Chem.* **2020**, *13*, 2001–2010. [[CrossRef](#)]
61. Suvina, V.; Krishna, S.M.; Nagaraju, D.; Melo, J.; Balakrishna, R.G. Polypyrrole-reduced graphene oxide nanocomposite hydrogels: A promising electrode material for the simultaneous detection of multiple heavy metal ions. *Mater. Lett.* **2018**, *232*, 209–212. [[CrossRef](#)]
62. Lo, M.; Seydou, M.; Bensaïda, A.; Pires, R.; Gningue-Sall, D.; Aaron, J.-J.; Mekhalif, Z.; Delhalle, J.; Chehimi, M.M. Polypyrrole-wrapped carbon nanotube composite films coated on diazonium-modified flexible ITO sheets for the electroanalysis of heavy metal ions. *Sensors* **2020**, *20*, 580. [[CrossRef](#)]
63. Lo, M.; Diaw, A.K.; Gningue-Sall, D.; Aaron, J.-J.; Oturan, M.A.; Chehimi, M.M. The role of diazonium interface chemistry in the design of high performance polypyrrole-coated flexible ITO sensing electrodes. *Electrochem. Commun.* **2017**, *77*, 14–18. [[CrossRef](#)]
64. Pineda, E.G.; Presa, M.R.; Gervasi, C.; Bolzán, A. Tubular-structured polypyrrole electrodes decorated with gold nanoparticles for electrochemical sensing. *J. Electroanal. Chem.* **2018**, *812*, 28–36. [[CrossRef](#)]
65. Xing, L.; Rong, Q.; Ma, Z. Non-enzymatic electrochemical sensing of hydrogen peroxide based on polypyrrole/platinum nanocomposites. *Sens. Actuators B Chem.* **2015**, *221*, 242–247. [[CrossRef](#)]
66. Gao, Y.-S.; Xu, J.-K.; Lu, L.-M.; Wu, L.-P.; Zhang, K.-X.; Nie, T.; Zhu, X.-F.; Wu, Y. Overoxidized polypyrrole/graphene nanocomposite with good electrochemical performance as novel electrode material for the detection of adenine and guanine. *Biosens. Bioelectron.* **2014**, *62*, 261–267. [[CrossRef](#)] [[PubMed](#)]

67. Armbruster, D.A.; Pry, T. Limit of blank, limit of detection and limit of quantitation. *Clin. Biochem. Rev.* **2008**, *29*, S49. [[PubMed](#)]
68. Guider, R.; Gandolfi, D.; Chalyan, T.; Pasquardini, L.; Samusenko, A.; Pederzoli, C.; Pucker, G.; Pavesi, L. Sensitivity and Limit of Detection of biosensors based on ring resonators. *Sens. Bio-Sens. Res.* **2015**, *6*, 99–102. [[CrossRef](#)]
69. Simões, F.R.; Xavier, M.G. Electrochemical Sensors. *Nanosci. Appl.* **2016**, 155–178.
70. Rashid, J.I.A.; Kannan, V.; Ahmad, M.H.; Mon, A.A.; Taufik, S.; Miskon, A.; Khim, O.K.; Yusof, N.A. An electrochemical sensor based on gold nanoparticles-functionalized reduced Graphene oxide screen printed electrode for the detection of Pyocyanin biomarker in Pseudomonas aeruginosa infection. *Mater. Sci. Eng. C* **2020**, *120*, 111625. [[CrossRef](#)] [[PubMed](#)]
71. Brett, A.M.O. Electrochemistry for probing DNA damage. In *Encyclopeida of Sensors*; Grimes, C.A., Dickey, E.C., Pishko, M.V., Eds.; American Scientific Publishers: Stevenson Ranch, CA, USA, 2006; pp. 1–14.
72. Brett, C.; Oliveira Brett, A.M. *Electrochemistry: Principles, Methods, and Applications*; Oxford University Press: New York, NY, USA, 1993.
73. De Souza, D.; Machado, S.; Avaca, L. Square wave voltammetry. Part 1: Theoretical aspects. *Quim. Nova* **2003**, *26*, 81–89.
74. Marie, M.; Mandal, S.; Manasreh, O. An electrochemical glucose sensor based on zinc oxide nanorods. *Sensors* **2015**, *15*, 18714–18723. [[CrossRef](#)]
75. Salunke, R.S.; Kasar, C.K.; Bangar, M.A.; Chavan, P.G.; Shirale, D.J. Electrodeposition of gold nanoparticles decorated single polypyrrole nanowire for arsenic detection in potable water: A chemiresistive sensor device. *J. Mater. Sci. Mater. Electron.* **2017**, *28*, 14672–14677. [[CrossRef](#)]
76. Hughes, W.T.; Shenep, J.L.; Rodman, J.H.; Fridland, A.; Willoughby, R.; Blanchard, S.; Purdue, L.; Coakley, D.F.; Cundy, K.C.; Culnane, M. Single-dose pharmacokinetics and safety of the oral antiviral compound adefovir dipivoxil in children infected with human immunodeficiency virus type 1. *Antimicrob. Agents Chemother.* **2000**, *44*, 1041–1046. [[CrossRef](#)] [[PubMed](#)]
77. Jain, R.; Sharma, R. Voltammetric quantification of anti-hepatitis drug Adefovir in biological matrix and pharmaceutical formulation. *J. Pharm. Anal.* **2012**, *2*, 98–104. [[CrossRef](#)] [[PubMed](#)]
78. Wang, S.; Lu, S.; Zhao, J.; Ye, J.; Huang, J.; Yang, X. An electric potential modulated cascade of catalyzed hairpin assembly and rolling chain amplification for microRNA detection. *Biosens. Bioelectron.* **2019**, *126*, 565–571. [[CrossRef](#)]
79. Low, S.S.; Pan, Y.; Ji, D.; Li, Y.; Lu, Y.; He, Y.; Chen, Q.; Liu, Q. Smartphone-based portable electrochemical biosensing system for detection of circulating microRNA-21 in saliva as a proof-of-concept. *Sens. Actuators B Chem.* **2020**, *308*, 127718.
80. Chan, H.-N.; Ho, S.-L.; He, D.; Li, H.-W. Direct and sensitive detection of circulating miRNA in human serum by ligase-mediated amplification. *Talanta* **2020**, *206*, 120217. [[CrossRef](#)]
81. He, C.; Chen, S.; Zhao, J.; Tian, J.; Zhao, S. Ultrasensitive detection of microRNA-21 based on electrophoresis assisted cascade chemiluminescence signal amplification for the identification of cancer cells. *Talanta* **2020**, *209*, 120505. [[CrossRef](#)]
82. Plausinaitis, D.; Sinkevicius, L.; Samukaite-Bubniene, U.; Ratautaite, V.; Ramanavicius, A. Evaluation of electrochemical quartz crystal microbalance based sensor modified by uric acid-imprinted polypyrrole. *Talanta* **2020**, *220*, 121414. [[CrossRef](#)] [[PubMed](#)]
83. Qi, R.; Lin, X.; Dai, J.; Zhao, H.; Liu, S.; Fei, T.; Zhang, T. Humidity sensors based on MCM-41/polypyrrole hybrid film via in-situ polymerization. *Sens. Actuators B Chem.* **2018**, *277*, 584–590. [[CrossRef](#)]